Part 2:
Observational evidence of winds

https://doi.org/10.1017/S1743921322003714 Published online by Cambridge University Press

Winds of Stars and Exoplanets
Proceedings IAU Symposium No. 370, 2023
A. A. Vidotto, L. Fossati & J. S. Vink, eds.
doi:10.1017/S1743921322003714

Observations of Winds and CMEs of Low-Mass Stars

Rachel A. Osten[1,2]

[1]Space Telescope Science Institute, Baltimore MD USA

[2]Center for Astrophysical Sciences, Department of Physics and Astronomy, Johns Hopkins University, Baltimore MD USA

Abstract. In this invited review talk I summarize some of the recent observational advances in understanding mass loss from low-mass stars. This can take the form of a relatively steady wind, or stochastically occurring coronal mass ejections (CMEs). In recent years, there has been an expansion of observational signatures used to probe mass loss in low-mass stars. These observational tools span the electromagnetic spectrum. There has also been a resurgence of interest in this topic because of its potential impact on exoplanet space weather and habitability. The numerous recent observational and theoretical results also point to the complexities involved, rather than using simple scalings from solar understanding. This underscores the need to understand reconnection and eruption processes on magnetically active stars as a tool to putting our Sun in context.

Keywords. stars: low-mass, stars: mass loss, stars: flare

1. Introduction

One of the exciting parts of attending a symposium like this one is the opportunity for cross-disciplinary interactions. The solar/stellar "connection" can often feel more like a great rift, when one compares and contrasts studies of the Sun with those of low-mass stars. Observations of the Sun will always win compared to stars in terms of spatial, spectral, and temporal resolution, as it's impossible to beat the harsh reality of a $1/d^2$ sensitivity function. Because of its centrality to life on Earth, the Sun is studied in exquisite detail, with daily global monitoring of its surface and near-solar environment, as well as a multi-wavelength context for interpreting many events on the Sun thanks to the constellation of ground- and space-based heliophysics measurements that exist. On the other hand, it is only one star studied at one point in its evolutionary sequence. Given recent progress in understanding the Sun in the context of other Sun-like stars, the Sun may even be unusual in where it sits in activity space, with evidence of the Sun sitting in transition between two cycle types (Metcalfe & van Saders 2017). G stars additionally are not representative of most of the stars in our galaxy. Given the wealth of detail we have in observations and understanding of the Sun and particularly magnetic activity-related phenomena, it is a worthwhile question to ask how universal are the processes occurring in this one star, and whether they might manifest differently in stars of differing characteristics. In contrast, low-mass M dwarfs are the most type of star in our Galaxy. While we cannot as yet spatially resolve these stars, they more than make up for this in the number which can be studied, and the span of ages, rotation rates and evolutionary histories that provide a broad range of parameter space. Admittedly, observations are typically fairly sparse, with little multi-wavelength context. Stellar astronomers also need to compete with the rest of the universe for observing time and funding!

Stellar mass-loss affects the interaction between a planet and its host star. On a larger scale, stellar mass-loss shapes the interaction between the heliosphere and the interstellar medium. In the last several years, with the rise in number of exoplanets detected outside of our solar system, it has become increasingly more topical to examine the likely impacts of space weather experienced by these exoplanets in their varieties of configurations.

The Sun currently has a feeble mass-loss rate, $\approx 2\times10^{-14}$ $M_\odot$ yr^{-1}, especially in comparison to the high rates experienced by massive O and B stars, which can be up to 10^9 times stronger. Because of this it has been difficult to make progress in observational constraints on measuring the mass-loss rates of nearby and solar-like stars.

In this review I'll deal with observational signatures of winds separately from those of transient coronal mass ejections. I recognize that the limit of CMEs occurring frequently enough will provide an integrated signature that should mimic that of a fast stellar wind, and address this when necessary. Because of the dynamic relationship between open and closed field lines during an eruptive, and the connection of CMEs with flares, I will also take a bit of an interlude to discuss connections between stellar winds, stellar flares, and CMEs.

2. Observational signatures of stellar winds in low-mass stars

Noting that the first detection of the solar wind was from in-situ particle measurements (Neugebauer & Snyder 1962), it is clear that astronomers need to be creative in searching for observational signatures of these winds. There are currently three main methods used to provide such observational constraints: excess absorption in the blueward wing of the Hydrogen Lyman α line; radio bremsstrahlung emission from the escaping material; and X-ray scattering from charge exchange emission. The use of exoplanets as test particles to diagnose stellar flows is also now possible with the rise of detections of exoplanets close in to their parent star, such as in Villarreal D'Angelo et al. (2021).

2.1. *Hydrogen Lyman alpha*

Hydrogen is the most abundant element in the universe and easily experiences absorption due to intervening material between us and astronomical objects. Pioneering work using high-resolution spectroscopic measurements of the Hydrogen Lyman alpha transition towards a sample of nearby stars (Wood 2004) revealed evidence for excess absorption on the short wavelength side of the Hydrogen Lyman alpha transition at 1216 Å, after accounting for the impact of absorption on this transition by passage through the interstellar medium. Figure 1 illustrates the geometry, including extra redward absorption of the Lyman alpha transition by material in our heliosphere's hydrogen wall. This method is currently the main method used to produce constraints on steady stellar winds in the cool half of the main sequence. It can only be done with high resolution ultraviolet spectroscopy from space. The Space Telescope Imaging Spectrograph on the Hubble Space Telescope currently corners the market on such observations, a situation that will remain until a true successor to HST's high resolution UV spectroscopic capabilities is launched sometime in the next two decades.

Wood and his collaborators use the word "astrosphere" to describe these detections, in parallel with the heliosphere in our solar system. The method does not detect the stellar wind itself, but rather the bow shock created when the wind interacts with the local interstellar medium. Detection of astrospheric absorption by itself does not provide a measurement of a stellar wind; this must be combined with models which describe the local flow of interstellar medium and assumptions about the gas in the astrosphere in order to arrive at a mass-loss rate. While there have been a range of

https://doi.org/10.1017/S1743921322003714 Published online by Cambridge University Press

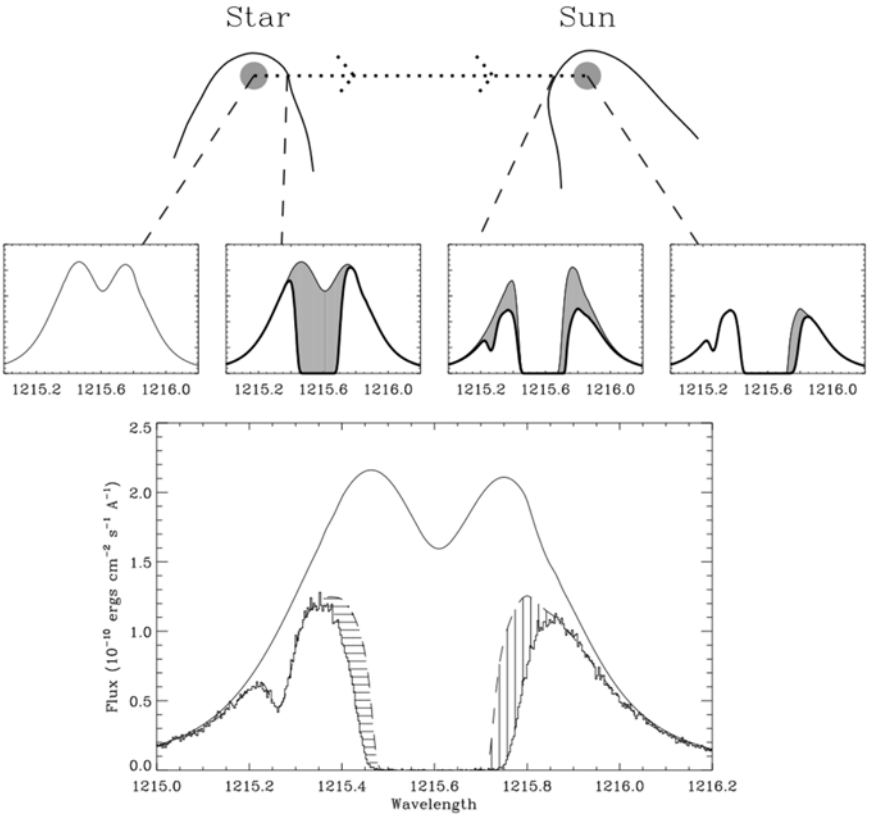

Figure 1. Figure 6 from Wood (2004) illustrating the geometry of astrospheric absorption and its impact on various parts of the Hydrogen Lyman α line profile. The top panel indicates sources of emission and absorption: Lyman α emission from the star, absorption first by its astrosphere, then from passage through the interstellar medium, and finally passage through the heliosphere on its way to being detected around the Earth. The middle panel delineates the spectral signature of each of these, while the profile on the bottom combines all of these effects. In the bottom plot, the thin black line shows the reconstructed intrinsic chromospheric emission from the star; the dashed line indicates the attenuation due to the ISM. The horizontally lined fill area to the left of line center indicates excess absorption from the astrosphere, and vertically lined fill area to the right of line center represents redward absorption from our own heliosphere. The underlying histogram is the resultant observed spectrum.

results, the most surprising thing about these measurements has been a general lack of evidence for significantly increased mass-loss rates in active stars.

A compilation of recent results from Wood et al. (2021) shows a good correlation between the surface X-ray flux of a sample of stars with detected astrospheres and the implied mass loss per unit surface area (Figure 2). X-ray coronal emission derives from closed magnetic field regions, whereas the stellar wind derives from open field regions. Given the large spread in the trend, it is clear that coronal activity and spectral type alone do not determine wind properties. Coronal mass ejections (described in more detail below) are one specific example of stochastically occurring transient stellar mass loss; for a star with a high enough rate of flares and associated coronal mass ejections, the integrated signature of such a CME-dominated wind should appear as a fast, dense stellar wind. That there is an inconsistency between what would be expected from extrapolating from the solar flare/CME occurrence relations and the winds observed on stars with known high rates of flaring suggests more complexity to the problem.

https://doi.org/10.1017/S1743921322003714 Published online by Cambridge University Press

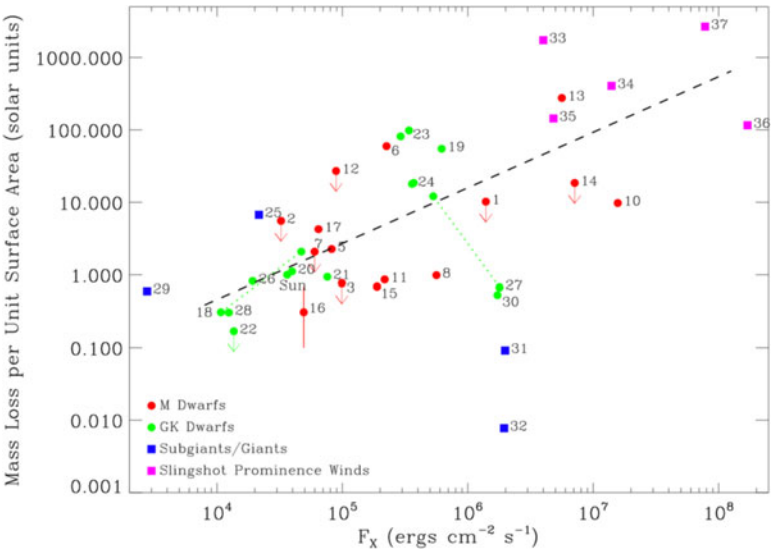

Figure 2. Figure 10 from Wood et al. (2021) summarizing recent measurements of steady mass loss from a variety of cool stars. Red and green circles, as well as blue squares indicate mass loss inferences from astrospheric detections, while fuschia squares come from slingshot prominence winds. The inferred mass loss rate per unit surface area appears to increase with surface X-ray flux, albeit with a large scatter.

2.2. *Radio Bremsstrahlung*

For a homogeneous plasma outflowing from a central star, incoherent radio emission can be detected via bremsstrahlung processes, with well-known flux-frequency $F_\nu \propto \nu^{-2}$ behavior in the optically thin regime, and a flat spectral dependence in the optically thick regime (Dulk 1985). Due to the orders of magnitude higher amounts of mass being lost in hot, massive stars, this detection technique has been most successful at providing constraints in the upper left part of the HR diagram, although recent investigations have probed the sensitivity of mass-loss from solar analogs under a range of assumptions about the directivity of the stellar wind (Fichtinger et al. 2017). This method can return constraints on mass-loss given a flux detection and assumptions about the temperature of the stellar wind; upper limits can provide useful constraints in contrast to the Lyman α method. The expected increase in sensitivity in future radio telescopes such as the next generation Very Large Array, along with an emphasis on frequencies higher than microwave regions, will enable constraints or detections of a number of the closest solar-neighborhood M dwarfs (Figure 3).

2.3. *X-ray scattering from charge exchange emission*

Wargelin & Drake (2001) proposed the use of X-ray scattering from charge exchange emission of astrospheric material with the interstellar medium as a method to provide constraints on stellar mass loss. For the nearest star outside our solar system, Proxima, they could provide limits on the mass loss rate via constraints on the amount of extended X-ray emission from the point source. For stars which are nearby and have a high enough inferred mass loss rate, detecting extended X-ray emission which has the spectral energy distribution expected from charge-exchange emission (which peaks at low X-ray energies) is a potentially viable tool for these limited numbers of objects.

https://doi.org/10.1017/S1743921322003714 Published online by Cambridge University Press

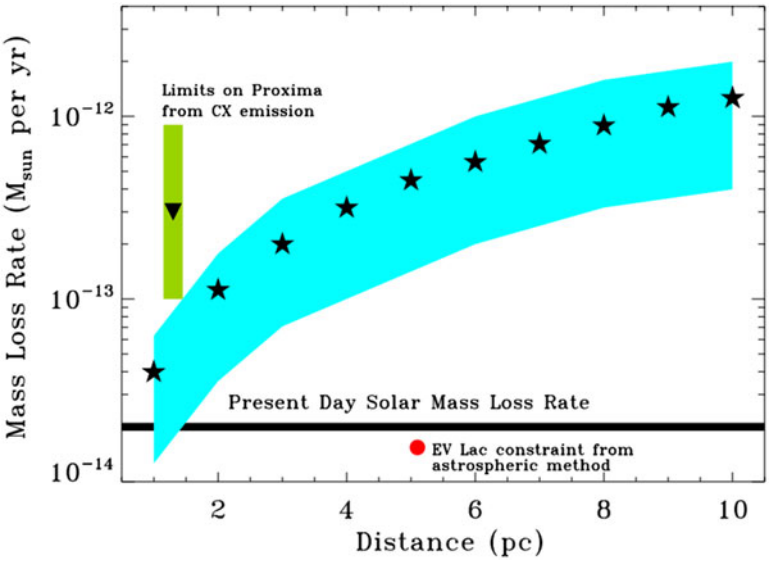

Figure 3. Grasp of the proposed next generation Very Large Array (ngVLA) for studying mass loss from nearby M dwarfs; Figure 3 from a community studies report by Osten & Crosley (2017). Constraints on mass loss rate are determined from the sensitivity imparted from a 12 hour observation, observing at 28 GHz, for a coronal wind with a range of wind speeds from 200–1000 km/s. The limits on mass loss from Proxima due to upper limits on charge exchange emission are indicated with the downward facing arrow and green rectangle. The red circle indicates the constraint on mass loss from the nearby flare star EV Lac obtained using the astrospheric method.

3. Connections between winds, flares, CMEs

As noted earlier, the source region on the disk of the Sun for wind emission is generally open magnetic fields, which allow mass and angular momentum to be lost to the system. X-ray emission and most observational signatures of stellar magnetic activity originates largely from closed-field regions. Magnetic reconnection flares, including coronal mass ejections, are a cross-over between these two regimes, as flares and CMEs involve the temporary opening of field lines as material is expelled away from the star. With the advent of high precision long timescale stellar photometry for the purpose of identifying transiting planets, it is relatively easy to identify and study stellar flares. Because of the positive correlation between many markers of magnetic activity, including flares, and the solar trend for a positive correlation between flares and CMEs, it is important to consider flare events in this discussion of mass loss. There are a few questions that arise in this context that must be considered to advance understanding of stellar mass loss in low-mass stars.

3.1. *How do flares in different wavelength regions relate to each other?*

The standard picture of magnetic reconnection flares (Benz & Güdel 2010) involves all layers of the stellar atmosphere, from the rarefied corona to the dense photosphere, and includes a variety of different physical processes, from plasma heating to particle acceleration and mass motions. The general assumption is that the emission mechanisms produced in separate layers of the stellar atmosphere are related to each other via the flare mechanism. However, even on the Sun correlations are not universal. As pointed out in Osten & Wolk (2015) the optical and X-ray flare frequency distributions for several well-studied M dwarfs show a general agreement in the index used to characterize the

https://doi.org/10.1017/S1743921322003714 Published online by Cambridge University Press

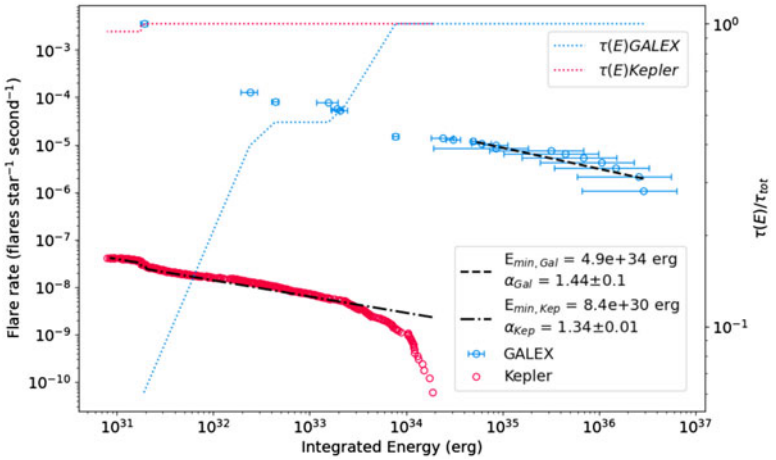

Figure 4. Figure from Brasseur et al. (submitted) illustrating the flare frequency distributions for a sample of twelve stars observed to flare in both Kepler (red circles) white-light and GALEX (blue circles) Near Ultraviolet bandpasses. The integrated energy on the abscissa is in the relevant bandpass. The dashed and dash-dotted lines are fits to the flare frequency distribution parameterized as a power-law. The flares are not simultaneous, yet the index of each distribution is remarkably similar, and suggestive of a common flare energy partition. The dotted lines and axis on the right side indicate the completeness of each dataset, namely the percentage of time where flares of energy E could have been detected based on the minimum detectable energy for that object.

flare frequency, assuming the cumulative flare rate decays as flare energy to the power $-\alpha$. The ultraviolet spectral region is especially important to characterize due to the huge impulsive flare increases seen in this portion of the electromagnetic spectrum, along with the impact on biological systems.

Recent work by Brasseur et al. (2023) uses a unique dataset of constraints from white-light flare measurements via the Kepler spacecraft, and near ultraviolet measurements with the GALEX spacecraft, to put constraints on the energy partition between these two bandpasses. From a sample of 12 stars observed to flare in both wavelength regions, but not simultaneously, we see the same conclusion as noted above from Osten & Wolk: the index of the flare frequency distributions of the two bandpasses are within the errors (Figure 4). This suggests that the offset between the two distributions could potentially be aligned with an common energy partition to convert from energy in a given bandpass to a bolometric flare energy partition.

The more tantalizing result in Brasseur et al. (2023) lies in the strictly simultaneous flare measurements. For over 1500 flares observed in the near UV, there are measurements obtained with the Kepler spacecraft. Curiously, there is no evidence for flare enhancements in the white-light portion of the spectrum to accompany the impulsive NUV flares, whose properties were largely studied in Brasseur et al. (2019). Figure 5 plots the NUV flare energy on the abscissa, with the ordinate displaying the upper limit of the Kepler to GALEX flare energy. That is, the ratio shows the energy of the largest Kepler band flare that would not have been detected at the time of the GALEX flare, to the observed NUV GALEX flare energy. This ratio shows a large scatter over four orders of magnitude, with evidence of a systematic trend with NUV flare energy. The few targetted multi-wavelength flare campaigns of nearby M dwarfs, shown with reddish-purple symbols in the figure, display a much narrower range of bandpass ratios which are more in line with what is expected from state-of-the-art radiative hydrodynamic models to describe the response of the atmosphere to the input of a range of electron beams.

https://doi.org/10.1017/S1743921322003714 Published online by Cambridge University Press

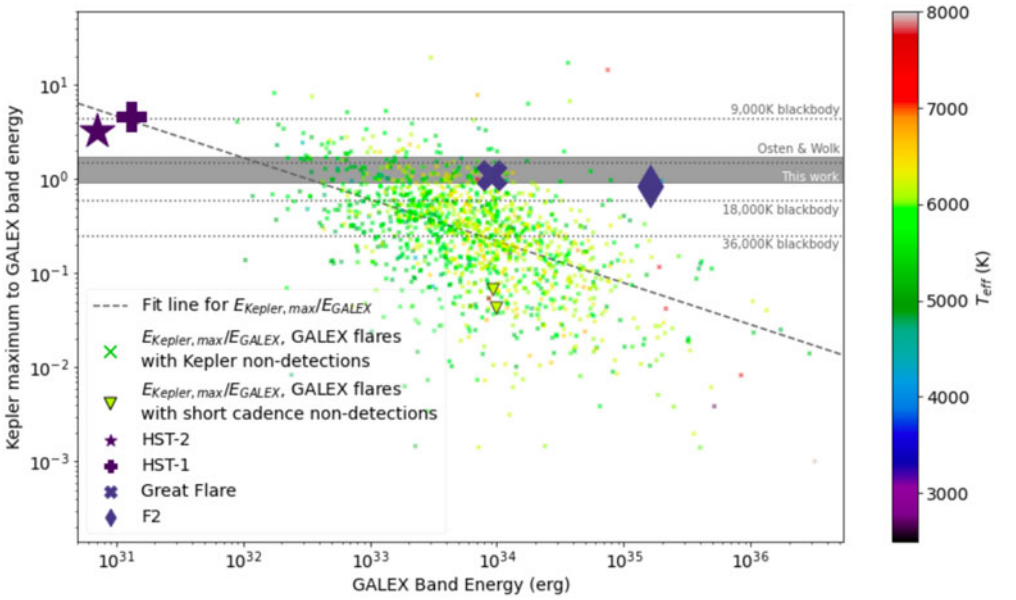

Figure 5. Figure from Brasseur et al. (submitted) indicating the spread of constraints on observed flare energy fractionation for a sample of 1559 datasets with simultaneous Kepler and GALEX measurements. The ordinate is the limit between the maximum undetected optical flare energy from Kepler data and the corresponding measured NUV flare energy. The abscissa is the measured NUV flare energy. The vast majority of the points come from long cadence Kepler data, while the two downward pointing triangles provide deeper constraints from short-cadence Kepler data. The dashed line is a fit to the data, indicating systematic dependence on increasing flare energy. The points are color-coded by the stellar effective temperature. Reddish-purple points are taken from literature studies of multi-wavelength flare campaigns on M dwarfs which place constraints on the NUV to optical flare energy ratios. Horizontal dotted lines are energy fractionations implied by a series of blackbody curves of given temperatures, or the fractionation described in Osten & Wolk (2015). The grey shaded area indicates the range of expected flare energy fractionations using radiative hydrodynamic models of the response of a flaring atmosphere to the input of energy from accelerated particles. These models tend to work better for M dwarf flares than for the range of superflares seen here on G and K stars.

3.2. *Are all flares part of eruptive events?*

As noted previously, on the Sun there is a good correspondence between the most energetic flare events and large coronal mass ejections. These relations have been developed by Emslie et al. (2012) relating the kinetic and potential energy of the CME to the bolometric radiated flare energy, and demonstrated by Drake et al. (2013) between the CME kinetic energy and an assumed partition between X-ray flare energies and bolometric flare energies. For both, the energy of the CME is 2–3 times that the total bolometric radiated flare energy. This led to a number of papers exploring the influence of flare-associated transient mass loss (e.g. Aarnio et al. 2013; Drake et al. 2013; Osten & Wolk 2015; Odert et al. 2017). The general result of these studies was an astoundingly high value of stellar mass loss for active stars, much higher than values inferred from models or from astrospheric detections of time-integrated mass loss.

So while the Sun shows good evidence for such correlations, extrapolating this result to the much higher energy flares observed on active stars produced results seemingly in contradiction with other techniques. There are a few supporting examples from the Sun itself, which occurred when a large active region produced a barrage of highly energetic X-ray flares with no accompanying eruptions. The explanations put forward by Zuccarello

https://doi.org/10.1017/S1743921322003714 Published online by Cambridge University Press

et al. (2014) invoking the torus instability have a nice potential to explain the stellar cases. Several papers by now have investigated a potential work-around to this, recognizing that magnetically active stars often have large magnetic fields overlying active regions. Alvarado-Gómez et al. (2018) demonstrated through modelling that such large field strengths can confine the plasma and prevent an eruption from happening.

4. Observational signatures of CMEs in low-mass stars

Coronal mass ejections are now recognized as one part of a solar eruptive event, which comprises a flare, the CME, and possibly solar energetic particles. While flares on stars outside our solar system have been seen since the early days of the 20th century (Hertzsprung 1924), the search for signatures of transient stellar mass loss have often relied on interpretations of odd-looking flares. It has only been in the last several years, with the rise of interest in exoplanetary space weather and impact of stars' magnetic activity on planetary habitability, that many concerted efforts have converged to explore systematic behavior of potential CME signatures in stars. Similarly to the case for wind studies, here too astronomers need to be creative. The workhorse observational technique for studying solar CMEs is the coronagraph, which blots out the main disk of the Sun and enables observation of Thomson scattering of photospheric photons off coronal electrons to probe the structures and dynamics of these eruptions. The parameter space of current astronomical coronagraphs, vis. the requisite sensitivities and angular scales achievable, do not allow for such searches to take place as of yet. There have been several lines of study to demonstrate the existence of stellar CMEs, as well as provide a probe of the systematic behavior of such events.

4.1. *Type II Radio Bursts*

The lynchpin for a CME detection method is one that demonstrates the presence of the eruption and is not dependent on the presence of a flare. Type II radio bursts nicely fit this bill. This is a unique radio signature formed from a super-Alfvenic shock as the CME propagates through the stellar atmosphere. Because of the stratified nature of the atmosphere, observing frequency traces density in the atmosphere, and the observed drift rate of the signal in frequency and time depends on the exciter speed, observing frequency, and coronal scale height. Thus measurements of a drift rate can be used to constrain the propagation speed of the eruption. In a series of papers, Crosley et al. (2016); Crosley & Osten (2018a,b) explored numerous low-frequency radio observations of nearby highly active stars, to look for the existence of these bursts. After a total of 64 hours on a binary star with a high flaring rate (exceeding one flare per hour at and above large solar flare energies where there is a good correlation between solar flares and CMEs), there were no detections of bursts that resembled the expected properties of type II bursts. Simultaneous optical observations occurring with some of the radio data show the lack of correlation between optical flares and any radio activity in the dynamic spectrum (Figure 6). This breakdown suggests that either CMEs occurring with flares on active M dwarfs are a rare occurrence, or that the conditions needed to create the super-Alfvenic shocks are not present at the observing frequencies and distances from the star being probed. Thus the type II radio bursts are an unfulfilled as of yet potential for diagnosing stellar mass loss.

4.2. *High velocity outflows in optical lines and coronal lines*

Flaring regions have many different types of flows associated with them. Observations of large blue shifts in emission (generally larger than the escape velocity) have been

https://doi.org/10.1017/S1743921322003714 Published online by Cambridge University Press

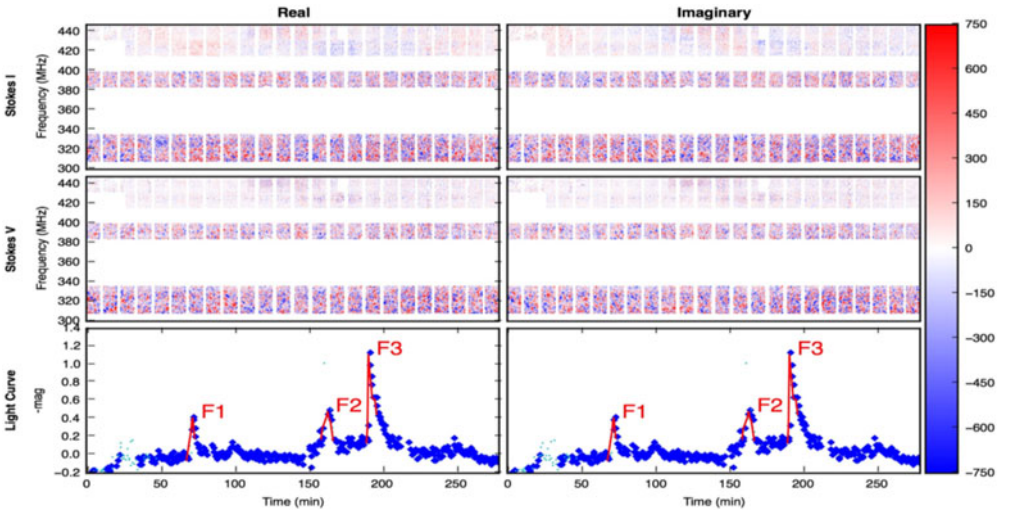

Figure 6. Figure 3 from Crosley & Osten (2018a) showing the radio dynamic spectrum (real and imaginary flux density as a function of frequency and time) of the binary EQ Peg, during a period of time when multiple optical flares were occurring (U-band light curve is the blue curve at the bottom). There is no evidence for radio bursts with signatures expected from passage of a super-Alfvenic shock produced by a CME travelling outward through the atmosphere. The total of 64 hours of observations, together with the flaring rate implying more than one flare per hour above an energy similar to solar flares where there is a nearly one to one correspondence between flares and CMEs, suggests either a breakdown in the flare-CME occurrence for highly active M dwarfs, or the inability of the CME to produce a shock at these observing frequencies sufficient to be detected.

interpreted as evidence of high velocity outflows attributable to an eruption or ejection. Argiroffi et al. (2019) detected an outflow in the lowest temperatures of coronal emission during a flare event on the cool giant HR9024 observed with the Chandra X-ray Observatory. Because this star is evolved, its escape velocity is lower than solar, and the blueshift of ∼90 km/s was seen only in emission lines of Oxygen, and only during the decay phase of the flare. They interpreted this as plausible evidence of a coronal mass ejection. More recently, Chen et al. (2022) reported on X-ray observations of the nearby flare star EV Lac, finding evidence for blue-shifted emission in lines of helium-like Oxygen (but not at higher temperatures), however below the escape velocity. They hesitated to call this evidence for a coronal mass ejection.

While X-ray observations of stars with sufficient spectral resolution and sensitivity do not occur often enough to be able to place limits on the occurrence rate of coronal flows associated with flares, optical observations of chromospheric lines enable longer term monitoring and more constraints. Maehara et al. (2021) reported on a sample of M dwarf flares, finding that only one out of 4 Hα-observed flares were associated with blue-ward asymmetries. of them exhibited blue shifts of some magnitude. Namekata et al. (2021) detected blueshifted emission as well as Hα absorption during a superflare on the solar-type star EK Dra. They interpreted this as an eruptive filament (Figure 7).

4.3. *Mass-loss dimming signatures*

Mason et al. (2014) described the possibility of a few types of dimming measurements that might accompany CMEs. The first, mass-loss dimming, would occur after the ejection of mass from the star leads to a reduction in emission compared to before the eruptive event. Veronig et al. (2021) explored dimming signatures in X-ray and Extreme

https://doi.org/10.1017/S1743921322003714 Published online by Cambridge University Press

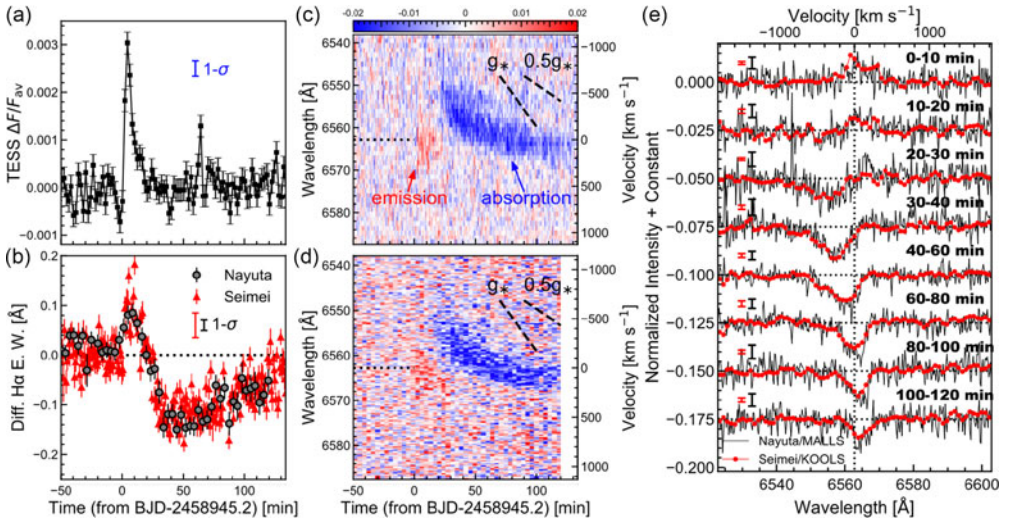

Figure 7. Figure 1 from Namekata et al. (2021) showing detection of an eruptive filament during a superflare on the solar-type star EK Dra. Left panels show TESS light curve at top, with differential Hα equivalent width variations during the time of the flare at bottom. The middle panel displays relative intensity as a function of time and wavelength. The right panel shows the Hα line profile integrated over the indicated time ranges, expressed in velocity space and wavelength. The vertical dashed line indicates line center. Blue-shifted absorption appears in the line profile immediately after the apparent cessation of the flare event.

Ultraviolet (EUV) light curves of magnetically active stars. They found several instances of large flares which were followed by a level of quiescent emission lower than that found immediately pre-flare. These observations were benchmarked by Sun-as-a-star EUV measurements. Because the quiescent emission levels of these stars show large variations, only strong dimming events can be identified. This technique does not enable determination of key parameters of the putative coronal mass emission like mass, velocity, height versus time. These have been seen in spatially resolved images of solar CMEs, and are also demonstrated in Sun-as-a-star high energy light curves tracing temperatures characteristic of the quiescent solar corona rather than flaring plasma (Harra et al. 2016). The geometry is illustrated schematically in Figure 8 left.

4.4. *X-ray absorption dimming*

Mason et al. (2014) also described the absorption dimming (Figure 8 right) phenomena as a possible signature of mass ejections. In this scenario, there is a temporary increase in absorption of the flaring region as absorbing material (here interpreted to be the expanding coronal mass ejection) moves across the line of sight. There have been a few detections of transient increases in absorbing column during large X-ray flares, most notably by Favata & Schmitt (1999). Moschou et al. (2017) used the results of the original fits to time-resolved spectroscopy from the flare on Algol described in Favata & Schmitt and modelled the trend of absorbing column with time as due to a self-similar expansion at constant velocity of a CME. This nicely explained the $N_H(t) \propto t^{-2}$ trend observed in the data. More recently, Osten et al. (in prep.) have been re-examining a sample of the largest stellar flares yet observed at X-ray wavelengths, and finding that many of these events are consistent with Hydrogen column density initially increasing, then decreasing with time during the decay of the flare. More work needs to be done to determine whether

https://doi.org/10.1017/S1743921322003714 Published online by Cambridge University Press

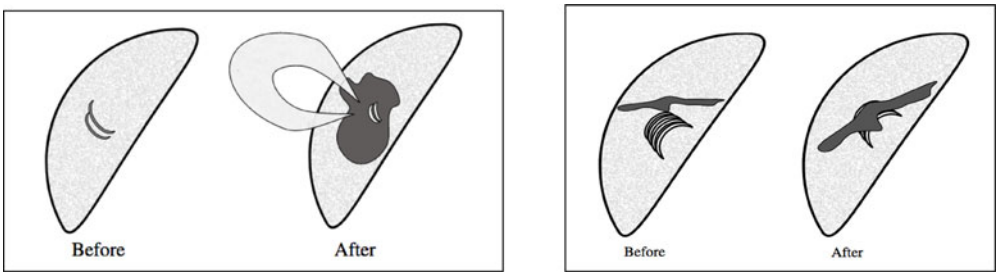

Figure 8. Figures 1 and 4 from Mason et al. (2014) pictorially explaining the circumstances surrounding two types of dimming potentially associated with coronal mass ejections. The left two panels indicate the situation before and after a mass-loss dimming event. Because of the evacuation of mass after the ejection event, there is less emitting material in the region compared to before the event, and differential measurements will indicate this as a decrease in emission. The right two panels indicate an absorption dimming event. Here, there is an arcade of flaring loops. As the ejected material expands it covers the lower-lying loop emission and provides a transient increase in the amount of absorption seen towards the line of sight to the flaring loops. With further expansion and associated decrease in column density, the amount of absorption will decrease back to a characteristic level. mass-loss dimming and absorption dimming.

these variations are in fact consistent with what would be expected from an ejection of mass from the corona.

5. Conclusions

The last several years have seen an expansion of observational signatures used to probe mass loss in low-mass stars. These techniques straddle the electromagnetic spectrum, and are beginning to return interesting insights into mass loss in cool stars. This activity will hopefully continue with the current suite of facilities as well as future facilities currently in development. There has been a concomitant expansion of interest in probing mass loss in low-mass stars. Part of this stems from a desire to deepen understanding of stellar astrophysics. With the rapid increase in the number of exoplanet detections, and the realization that close-in planets around low-mass stars will provide the first opportunities to study potentially habitable planets in the near future, it is more important than ever to understand the impact of stars on exoplanet space weather. Occurring along with these is an expansion of understanding of the complexities in extrapolating simple scalings from a solar understanding. This motivates the need to understand reconnection and eruption processes on magnetically active stars as a tool to putting our Sun in context.

References

Aarnio, A. N., Matt, S. P., & Stassun, K. G. 2013, Astronomische Nachrichten, 334, 77
Alvarado-Gómez, J. D., Drake, J. J., Cohen, O., Moschou, S. P., & Garraffo, C. 2018, ApJ, 862, 93
Argiroffi, C., Reale, F., Drake, J. J., Ciaravella, A., Testa, P., Bonito, R., Miceli, M., Orlando, S., & Peres, G. 2019, Nature Astronomy, 3, 742
Benz, A. O. & Güdel, M. 2010, ARA&A, 48, 241
Brasseur, C. E., Osten, R. A., & Fleming, S. W. 2019, ApJ, 883, 88
Brasseur et al. 2023, ApJ, 944, 5
Chen, H., Tian, H., Li, H., Wang, J., Lu, H., Xu, Y., Hou, Z., & Wu, Y. 2022, ApJ, 933, 92
Crosley, M. K. & Osten, R. A. 2018a, ApJ, 856, 39
—. 2018b, ApJ, 862, 113
Crosley, M. K., Osten, R. A., Broderick, J. W., Corbel, S., Eislöffel, J., Grießmeier, J. M., van Leeuwen, J., Rowlinson, A., Zarka, P., & Norman, C. 2016, ApJ, 830, 24
Drake, J. J., Cohen, O., Yashiro, S., & Gopalswamy, N. 2013, ApJ, 764, 170

https://doi.org/10.1017/S1743921322003714 Published online by Cambridge University Press

Dulk, G. A. 1985, ARA&A, 23, 169
Emslie, A. G., Dennis, B. R., Shih, A. Y., Chamberlin, P. C., Mewaldt, R. A., Moore, C. S., Share, G. H., Vourlidas, A., & Welsch, B. T. 2012, ApJ, 759, 71
Favata, F. & Schmitt, J. H. M. M. 1999, A&A, 350, 900
Fichtinger, B., Güdel, M., Mutel, R. L., Hallinan, G., Gaidos, E., Skinner, S. L., Lynch, C., & Gayley, K. G. 2017, A&A, 599, A127
Harra, L. K., Schrijver, C. J., Janvier, M., Toriumi, S., Hudson, H., Matthews, S., Woods, M. M., Hara, H., Guedel, M., Kowalski, A., Osten, R., Kusano, K., & Lueftinger, T. 2016, Solar Physics, 291, 1761
Hertzsprung, E. 1924, BAIN, 2, 87
Maehara, H., Notsu, Y., Namekata, K., Honda, S., Kowalski, A. F., Katoh, N., Ohshima, T., Iida, K., Oeda, M., Murata, K. L., Yamanaka, M., Takagi, K., Sasada, M., Akitaya, H., Ikuta, K., Okamoto, S., Nogami, D., & Shibata, K. 2021, PASJ, 73, 44
Mason, J. P., Woods, T. N., Caspi, A., Thompson, B. J., & Hock, R. A. 2014, ApJ, 789, 61
Metcalfe, T. S. & van Saders, J. 2017, Solar Physics, 292, 126
Moschou, S.-P., Drake, J. J., Cohen, O., Alvarado-Gomez, J. D., & Garraffo, C. 2017, ApJ, 850, 191
Namekata, K., Maehara, H., Honda, S., Notsu, Y., Okamoto, S., Takahashi, J., Takayama, M., Ohshima, T., Saito, T., Katoh, N., Tozuka, M., Murata, K. L., Ogawa, F., Niwano, M., Adachi, R., Oeda, M., Shiraishi, K., Isogai, K., Seki, D., Ishii, T. T., Ichimoto, K., Nogami, D., & Shibata, K. 2021, Nature Astronomy, 6, 241
Neugebauer, M. & Snyder, C. W. 1962, Science, 138, 1095
Odert, P., Leitzinger, M., Hanslmeier, A., & Lammer, H. 2017, MNRAS, 472, 876
Osten, R. A. & Crosley, M. K. 2017, arXiv e-prints, arXiv:1711.05113
Osten, R. A. & Wolk, S. J. 2015, ApJ, 809, 79
Veronig, A. M., Odert, P., Leitzinger, M., Dissauer, K., Fleck, N. C., & Hudson, H. S. 2021, Nature Astronomy, 5, 697
Villarreal D'Angelo, C., Vidotto, A. A., Esquivel, A., Hazra, G., & Youngblood, A. 2021, MNRAS, 501, 4383
Wargelin, B. J. & Drake, J. J. 2001, ApJ Letters, 546, L57
Wood, B. E. 2004, Living Reviews in Solar Physics, 1, 2
Wood, B. E., Müller, H.-R., Redfield, S., Konow, F., Vannier, H., Linsky, J. L., Youngblood, A., Vidotto, A. A., Jardine, M., Alvarado-Gómez, J. D., & Drake, J. J. 2021, ApJ, 915, 37
Zuccarello, F. P., Seaton, D. B., Mierla, M., Poedts, S., Rachmeler, L. A., Romano, P., & Zuccarello, F. 2014, ApJ, 785, 88